

Ab-initio calculations of the optical properties of the Si(113) 3×2 ADI surface

K. Gaál-Nagy* and G. Onida

European Theoretical Spectroscopy Facility (ETSF), CNISM-CNR-INFN,
and Dipartimento di Fisica dell'Università degli Studi di Milano, via Celoria 16, I-20133 Milano, Italy

(Dated: January 8, 2019)

We investigated the stable silicon (113) surface with a 3×2 ADI reconstruction by ab-initio methods. The ground state properties have been obtained using the density-functional theory. We present the dispersion of the electronic band structure, where the surface bands have been distinguished from the projected bulk bands by calculating their localization in the slab. The optical spectra, here the reflectance anisotropy (RAS), have been obtained within the independent particle random phase approximation. We identified surface features in the spectra tracing them back to the responsible electronic states and, studied their localization in the slab. A comparison with available experimental data for the band structure and the RAS shows a good agreement.

PACS numbers: 78.68.+m 68.35.Bs 73.20.At

I. INTRODUCTION

Although being of high index, the vicinal Si(113) surface is one of the stable silicon (Si) surfaces.¹ This surface is of technological interest, since atomically smooth, ultrathin oxide films can be grown on it.² Hence, it is dealt as a candidate for the next generation of wafers,³ and has potential applications in nanostructures technology. Si(113) can be used as a substrate for the self-assembled growth of germanium (Ge) nanodots⁴ and nanowires^{5,6,7}, as well as Ge^{8,9} and SiGe¹⁰ islands. Besides the technological interest, Si(113) is also of fundamental one, because it shows phase transitions between its 3×2 and 3×1 reconstructions. These phase transitions can be induced by temperature^{11,12,13,14,15,16} and by contamination.^{17,18,19,20,21,22,23,24} The latter ones affect also the discussion about the surface reconstruction. In spite of the measurement of a 3×1 reconstruction,²⁵ most of the experiments show at room temperature (RT) a 3×2 surface periodicity.^{4,13,17,18,20,26,27,28,29} The finding of the 3×1 periodicity might be due to contamination¹⁷ and the 3×2 one is assumed as the surface unit of clean Si(113) at RT.

Various surface reconstructions have been proposed for the Si(113) 3×2 surface. The most probable surface model is the ADI (adatom-dimer-interstitial) reconstruction of Dąbrowski,³⁰ which is in agreement with experimental high-resolution transmission electron microscopy (HRTEM)^{31,32} and scanning tunneling microscopy (STM)^{4,13,26,27,30,33} images. It has been confirmed by other theoretical investigations, too.^{33,34,35,36} A top view of the surface unit cell is shown in Fig. 1. The surface reconstruction shows two adatoms, and two pentagons with a dimer along the $[1\bar{1}0]$ direction, with one pentagon hosting an interstitial atom in its center.

Earlier structured models were based on the structure proposed by Ranke,³⁷ Si(113) 3×1 AD, which is similar to the ADI one. It can be deduced from the ADI model by eliminating the interstitial atom and relaxing the atoms in z direction. Despite being intrinsically 3×1 , also in the 3×1 AD model the 3×2 periodicity can be obtained

either by canceling one pentagon in each 3×2 surface unit cell (“surface-void” [37]), or by manipulating the z coordinates of the pentagons in order to break the symmetry (“corrugated” [38], “puckered” [28,39], “shifted” [40], etc.). Since the 3×1 periodicity is also interesting for the phase transition, being the periodicity of the high-temperature phase, besides the 3×1 AD model also a 3×1 AI one, with an interstitial atom at each pentagon has been proposed.^{33,41} However, also other surface models have been assumed, generally based on the models of Ranke or Dąbrowski.^{42,43}

From the theoretical point of view, the most stable surface (i.e., the one with the lowest surface energy) should be selected. For some of the models above, the surface energy has been calculated, unfortunately by using different methods. There exist some studies assuming more than one surface reconstruction^{30,33,36,44,45} within the same framework, but none of them considered all available surface models for a comparison. Most of the

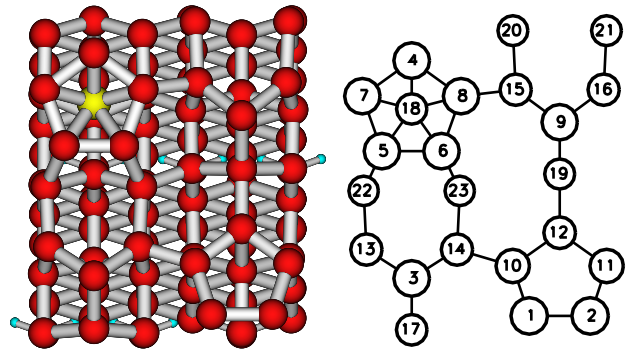


FIG. 1: (color online) Top view of the Si(113) 3×2 ADI cell (x, y plane corresponding to $[1\bar{1}0]$ and $[3\bar{3}2]$, respectively). Silicon atoms are in large dark spheres (red). The interstitial Si atom (atom 18) is depicted as a large light (yellow) sphere. Hydrogen atoms are small light spheres (blue). For a side view see Figs. 8 and 5. Surface atoms (see sketch) include two pentagons with dimers (atom pairs 1-2 and 5-6) and two adatoms (atoms 3 and 9).

calculations have shown that the Si(113)3×2ADI surface has the lowest surface energy with respect to the other assumed reconstructions.

Nevertheless, not all measurements agree with the ADI model.^{28,31,40} The main criticism to the ADI model is due to the presence of a mirror plane, which should yield the extinction of some diffraction reflections,⁴³ because the corresponding patterns have been seen in some experiment.⁴⁶ Thus, models different from the ADI one are also being considered and a final conclusion has not been drawn yet.

An alternative approach for surface investigations is given by the study of its optical properties. A very efficient technique is the reflectance anisotropy spectroscopy (RAS), which can be used in situ for the surface determination. The interpretation of such spectra is a demanding task. For this purpose it is necessary to have theoretical reference data together with a correlation of the spectral features and the surface reconstruction elements.

The RAS of the Si(113) surface has been measured since ten years.^{47,48} The first theoretical investigations of the RAS for the Si(113) surface has been performed in 1998 by using a dipole approximation for the ideal bulk atomic positions.⁴⁹ In the same year, a tight-binding calculation has been done for the Si(113)3×2ADI model.⁵⁰, where the bulk derivative-like peaks have been found with the wrong sign. Although tight-binding calculations yield good results for bulk silicon, the low-energy range of the spectra, which is related to the surface, is usually not described very well.⁵¹

For this purpose, we choose an ab-initio approach to investigate the optical properties of the Si(113) surface. The goal of this study is to find out whether surface-related structures in the spectra can be traced back to some characteristic surface reconstruction elements of Si(113)3×2ADI (pentagons, interstitial, adatoms, etc.), and which kind of changes can be predicted with respect to other surface models. In this way optical spectroscopy could be used to discriminate between different models for reconstruction of the Si(113) surface. Due to the wide acceptance of the Si(113)3×2ADI, we used this model as a starting point.

This article is organized as follows: After summarizing shortly the methods used for the calculation (Section II), we first focus on the ground state properties (Section III). Since the optical spectra are determined by the electronic transitions, an investigation of the electronic structure is presented in Section IV. A detailed discussion of the optical spectra is given in Section V, and, finally, we summarize and draw a conclusion.

II. METHOD

We have performed ab-initio total energy calculations using the periodic slab method within the framework of the density-functional theory⁵² (DFT) as implemented in the ABINIT⁵³ and TOSCA⁵⁴ packages.

For the exchange-correlation energy in the Kohn-Sham equations⁵⁵ the local-density approximation^{56,57} (LDA) has been chosen. The eigenfunctions have been expanded into plane waves using pseudopotentials, here normconserving ones in the Troullier-Martins style.⁵⁸

After converging the ground state structure with ABINIT, the optical properties have been calculated using the TOSCA package.⁵⁴ The probability $P_{v\mathbf{k},c\mathbf{k}}^j$ of the electronic transitions between the valence (v) and the conduction (c) states with electronic eigenenergies $E_{c\mathbf{k}}$ and $E_{v\mathbf{k}}$ for light polarized in j ($j = x, y, z$) direction at a given point \mathbf{k} in the reciprocal space has been calculated as the diagonal elements of the velocity operator.⁵⁹ Working within the independent particle random phase approximation⁶⁰ (IPRPA), local-field, self-energy, and excitonic effects are neglected. For our system we assume that they can be well described by the scissor operator approach,⁶¹ hence we stick to the IPRPA to describe the optical properties. In order to obtain the RAS, in a first step the imaginary part of the slab polarizability α^s has been calculated by

$$\text{Im}[4\pi\alpha_{jj}^s(\omega)] = \frac{8\pi^2 e^2}{m^2 \omega^2 A} \sum_{\mathbf{k}} \sum_{v,c} \left| P_{v\mathbf{k},c\mathbf{k}}^j \right|^2 \times \delta(E_{c\mathbf{k}} - E_{v\mathbf{k}} - \hbar\omega) \quad (1)$$

for an energy ω .⁶² Here, A is the surface area, m and e the electron mass and charge, respectively. In order to smooth the resulting spectra, a Gaussian broadening has been applied, because it leads to more well-defined structured spectra than the Lorentzian one. The RAS is defined as the difference of the deviation from the Fresnel reflectivity $\Delta R_j/R$ for the orthogonal polarizations within the surface plane (here the x and y direction):

$$\text{RAS} = \frac{\Delta R}{R} = \frac{\Delta R_x}{R} - \frac{\Delta R_y}{R} \quad (2)$$

The deviation from the Fresnel reflectivity for normal incident light is given by⁶²

$$\frac{\Delta R_j}{R} = 4 \left(\frac{\omega}{c_0} \right) \text{Im} \left[\frac{\alpha_{jj}^{\text{surf}}(\omega)}{\alpha_b(\omega)} \right], \quad (3)$$

where $\alpha_{jj}^{\text{surf}}$ is the complex surface polarizability and $\alpha_b(\omega)$ the bulk one (c_0 : velocity of light). The surface polarizability can be obtained by subtracting the bulk contribution from the slab one. Since the imaginary part is taken from the ratio, the bulk part in the numerator vanishes, and Eq. (3) holds also for α_{jj}^s , instead of $\alpha_{jj}^{\text{surf}}$. The complex polarizability function α is derived from the imaginary part via the Kramers-Kronig transform.

Finally, to keep into account the self-energy and excitonic effects in an approximative way, a scissor operator shift⁶¹ has been applied to the eigenenergies.

III. GROUND STATE

For our calculations we have chosen the cell with the 3×2 ADI surface reconstruction as described above. We have used slabs with 11 and 7 double layers (DL) of Si, respectively. The amount of vacuum was taken equal to the slab thickness. Each DL consists of 12 Si atoms, just the surface DL contains one atom less. Since the slab is not symmetric, the dangling bonds at the bottom of the slab have been saturated with hydrogen (H). Therefore, the cells contain 131 or 83 Si atoms, respectively, and 18 H atoms. A top view of the slab is shown in Fig.1, while the side views of the 11 DL cell can be seen in Figs. 5 and 8.

The convergence of the total energy requires 4 \mathbf{k} Monkhorst-Pack⁶³ points in the irreducible wedge of the Brillouin zone (IBZ), and a kinetic-energy cutoff of 16 Ry. With these parameters, the error in the total energy is less than 0.046 eV per atom.

A relaxation of the topmost 6 DL, computing the forces acting on the atoms (the remaining DL have been kept fixed to bulk positions) shows significant changes with respect to the bulk positions just in the topmost 4 DL. Therefore, these 4 DL have been optimized till the forces are less than 0.08 eV/Å.

We have calculated the surface energy by subtracting the energy of the hydrogenated surface and the bulk energy from the energy of the slab. The resulting value of 12.74 eV per unit cell agrees very well with the value of 12.69 eV obtained by Stekolnikov et al.⁴⁴ As a consequence, the value of surface energy per unit area of 87.87 meV/Å² is in good agreement with the one of Stekolnikov et al.⁴⁴ (87.36 meV/Å²). However, it is slightly lower than the ones obtained from other groups (97 meV/Å²[30,33], 90.4 meV/Å²[36], 94.8 meV/Å²[45]) using various methods. Nevertheless, it is lower than that for other surface reconstructions and the overall agreement is good.

IV. ELECTRONIC STRUCTURE

After the ground state has been converged, a first step towards the optical properties is an analysis of the electronic structure. We started with the calculation of the electronic density of states (DOS) as displayed in Fig. 2, where the highest occupied band (HOMO) is set to 0 eV. There, a comparison of the DOS calculated with the 7 DL and the 11 DL slab is shown. The DOS has been obtained using a Brillouin-zone summation over 25 \mathbf{k} points, together with a Gaussian broadening of 0.06 eV. The general shape is similar to the one of bulk silicon for the occupied bands. In addition, around the energy gap surface-related structures are visible: one strong peak at the conduction band edge and a peak with a shoulder and another shoulder close to the bulk-like part of the DOS at the valence band edge. The use of the 7 DL and the 11 DL supercell leads to just minor differences.

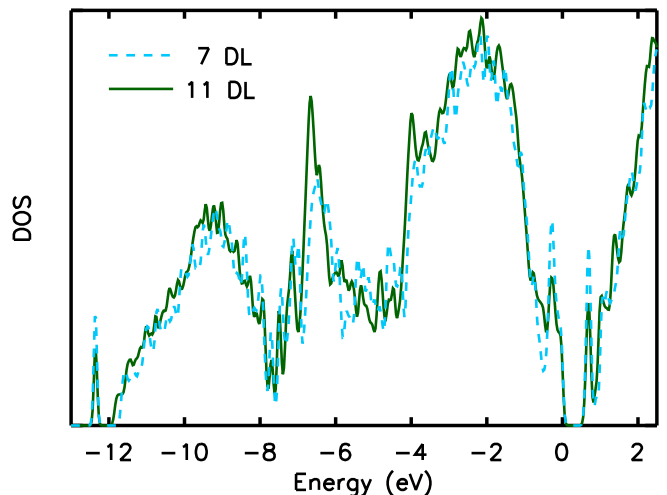


FIG. 2: (Color online) Electronic density of states for the 11 DL cell (solid dark-green lines) and the 7 DL cell (dashed light-blue lines). The zero of the energy scale is set to the top-valence state, and the height of the DOS is scaled with respect to the total number of atoms in the corresponding cell (see text).

By normalizing the DOS to the total number of atoms in the slab, the height of the surface peaks (around the gap) appears to be smaller for the thicker slab.

The valence peaks around the Fermi energy, which are in addition to the bulk DOS, have been also found experimentally and they correspond to surface bands. Using angle-resolved ultraviolet photoemission spectra (ARUPS) Myler and Jacobi¹⁸ found two peaks separated by 1.6 eV, where the second one is broad and could hide two single peaks. A similar experiment has been performed using angle-resolved photoelectron spectroscopy (ARPES) showing two single peaks separated by 0.4 eV, and a third one at lower energy with a non-dispersive character, which is not resolved in the other experiment.^{15,16,64} At normal emission, the two close peaks fall together resulting in a single broad peak, which has been found also by Myler and Jacobi.¹⁸ Thus, the surface peak around the HOMO in the DOS is well defined in the experiments, and it contains probably two peaks as indicated by the shoulder. Furthermore, the core level spectra of Hwang et al.^{15,16} were fitted using three surface peaks, where the second shoulder in our DOS might refer to that third peak. In scanning tunneling spectra (STS)⁶⁵ two peaks are visible. The low energy maximum has been attributed to the tetramers and the high energy maximum to the adatoms of the Si(113) 3×2 ADI reconstructed surface. For the peak at the lowest unoccupied band (LUMO), which should be accessible by inverse photoelectron spectroscopy, no experimental results exist.

After identifying the surface structures in the DOS we have investigated the dispersion of the electronic eigenenergies using the 11 DL supercell. The results are displayed in Fig. 3. In order to separate the surface bands from the bulk background we have calculated the local-

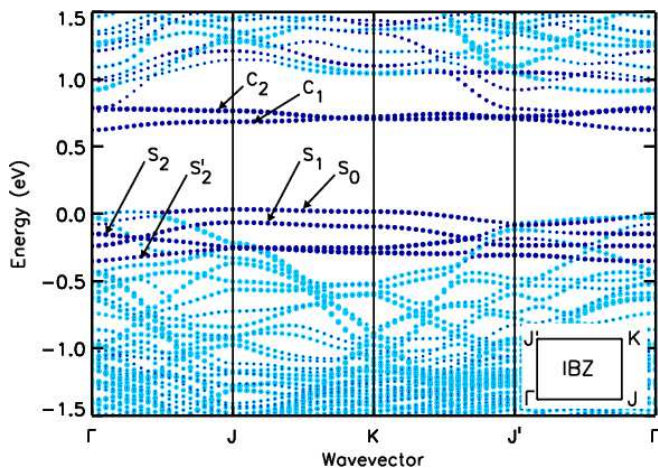


FIG. 3: (Color online) Dispersion of the electronic eigenenergies along the high-symmetry directions of the irreducible part of the Brillouin zone (IBZ). According to the localization of the corresponding states in the slab, light dots correspond to bulk states and dark ones to surface states. The dot size accords to the value obtained by Eq. (4) (see text).

ization L_n for each state n by

$$L_n = \int d\mathbf{r} \psi_{n\mathbf{k}}^*(\mathbf{r}) \theta(z) \psi_{n\mathbf{k}} \quad (4)$$

where $\theta(z)$ is a realspace boxcar function⁶⁶, meaning $\theta(z) = 1$ for a given range in z direction and zero otherwise. $\psi_{n\mathbf{k}}$ is the single band wave function for a given point \mathbf{k} and the integral is taken over the whole supercell. Considering the range, e.g., from the subsurface DL to the vacuum above, the value of L_n corresponds to the integrated charge for that state located in the x - y slice with the chosen z range. In this way, this value indicates the amount of localization in the range selected by $\theta(z)$.

Fig. 3 shows the results. The surface-localized bands are drawn with dark symbols (the z range has been chosen to cover the topmost two DLs), and the bulk-localized bands with light symbols (the z range has been chosen to cover the lowest seven DLs where the relaxation has not changed the bulk positions). The size of the dots corresponds to the amount of localization in this area. This means, e.g., for the topmost four valence bands at the Γ point, that the top band is less localized in the bulk area than the second one and the third band is less localized in the surface area than the fourth one.

With this procedure we have identified three surface valence bands (S_0 , S_1 , S_2) and two surface conduction bands (C_1 , C_2), as visible in Fig. 3. All surface bands show a partial overlap with the bulk band structure. This points to a reduced influence of excitonic effects, and thus, the IPRPA scissor approximation is expected to work well. The state S_2 appears as a state folded at J along the $[1\bar{1}0]$ direction, and hence shows 3×1 periodicity. The other surface states show the 3×2 one. Of course, the eigenvectors have 3×2 symmetry for all surface states due to the choice of the 3×2 supercell. In both

the experiments, ARUPS and ARPES, valence surface states with 3×1 and 3×2 periodicity have been found, but with a larger energy difference, which is here between J and K at about 0.16–0.19 eV. The shape of the bands S_1 and S_2 are in excellent agreement with the measured ones, and show a similar dispersion of about 0.17 eV and 0.20 eV, respectively, compared with the experiments of An et al.⁶⁴ (S_1 : 0.15 eV and S_2 : 0.30 eV) and Myler and Jacobi¹⁸ (S_1 : 0.20 eV and S_2 : 0.15 eV). Hence we conclude that these two states are the ones appearing in the experiments. Along the Γ -J direction the separation of the bands shows large variations within the two experiments, where we have here an overlap. The discrepancy might be due to the negligence of quasiparticle corrections as well as due to experimental setups. Considering available theoretical investigations of the dispersion of the eigenenergies of the Si(113) surface (besides the tight-binding study of Wang et al.³⁹ using a puckered surface model, which is hence not comparable), there exist just the investigation of Stekolnikov et al.³⁵. Within their results they obtain also the surface states S_0 and S_1 , where the S_2 might be hidden in the bulk-projected band structure. The energy spacing between these states is similar to the one obtained here.

By calculating the squared modulus of the wave functions of the surface states we have been able to localize them more precisely in the slab (see Fig. 4). The states S_0 and S_1 are located at the adatoms (atom 3 and atom 9, respectively, see Fig. 1) and show a dangling bond character, which is in agreement with the results of Ref. [35] and the assumption of Ref. [65]. The states C_1 and C_2 have been found at the atoms 4-7-8 and 5-6-7-8 of the pentagon with the interstitial, which is stated similarly in Ref. [35]. Furthermore, the surface state S_2 is located at one adatom and two atoms of the empty pentagon (atoms 1-2 and 3), which has not been inves-

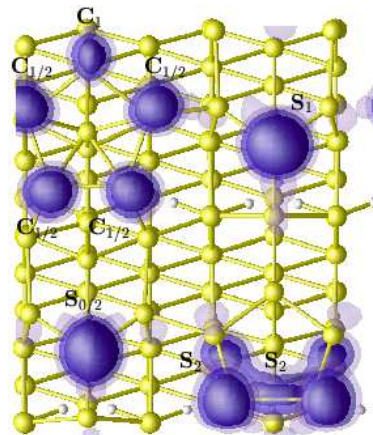


FIG. 4: (Color online): Top view (x - y side like Fig. 1) of the Si(113) 3×2 ADI cell together with the charge density of the surface states S_0 , S_1 , S_2 , C_1 , and C_2 (see text). Note the overlap between the localization of some of the surfaces states.

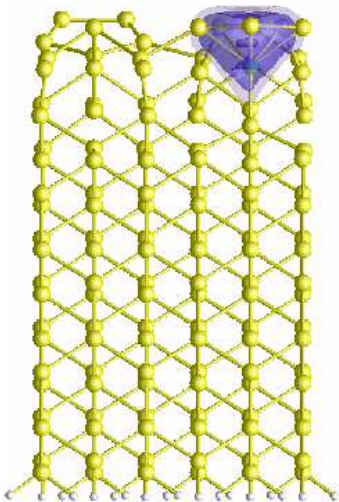


FIG. 5: (Color online): Side view (x - z plane) of the Si(113) 3×2 ADI cell together with the charge density of the low-energy Tamm-like state. Si atoms are drawn as large spheres, H atoms as small spheres.

tigated before. However, this was already assumed by Arabczyk et al.⁶⁵. Anyway, also this state is present in experimental^{4,26,27,30,33,36} and theoretical^{30,33,35,36} STM images.

Besides the surface states above, we have obtained an additional valence surface state at very low energy corresponding to the separated peak at around -12.5 eV in the DOS of Fig. 2. This state shows a dispersion of less than 16 meV, which follows the dispersion of the lowest valence states, which is 20 times larger. Thus, this nearly flat state can be considered as a Tamm-like state.⁶⁷ This state is located in between the atoms of the pentagon with interstitial (atoms 4-5-6-7-8 and 18), as displayed in Fig. 5. The large separation between these sites in the real space is responsible for the flat character of the band. However, it is not the first time that such a state has been found. Pandey et al.⁶⁸ found a flat surface band at low energy (≈ 10.8 eV) which is partially below the bulk valence bands for Si(111):SiH₃. Also a theoretical and experimental investigation of the GaAs(110) 1×1 surface⁶⁹ shows, that one surface state is located below the valence band minimum with a gap in between. The Tamm-like state found in our calculation should be accessible within measurements and its experimental finding would confirm the validity of the surface model used here. Due to its low-energy character, transitions from that state will not appear in the low or middle energy range of the RAS.

V. OPTICAL PROPERTIES

In this section we present results for the optical spectra, in particular for the RAS, of the Si(113) surface. We focus on the convergence with respect to the \mathbf{k} points

and the slab thickness, we analyze the RAS regarding surface contribution and responsible transitions, and we compare with available experimental results.

A. Convergence tests

For the optical properties we have performed convergence tests concerning the number of conduction states and the number of \mathbf{k} points used in Eq. (1). A number of 460 bands in total (189 conduction states) have been sufficient for the 11 DL cell as well as 360 bands (185 conduction states) for the 7 DL one, respectively. Each state has been expanded into plane waves. The use of 4000 \mathbf{G} vectors over the available set of ≈ 24000 plane waves has been enough for the convergence of the matrix elements. The convergence tests with respect to the special \mathbf{k} points are more demanding. In our case, the \mathbf{k} points can be chosen in one quarter of the BZ corresponding to the IBZ. A Gaussian broadening of 0.08 eV gives reasonably structured spectra. We have performed tests with various sets of \mathbf{k} points for the 7 DL cell as shown in Fig. 6. As visible in the figure, up to 25 \mathbf{k} points the spectra still show some deviations. With a single \mathbf{k} analysis⁷⁰ it has been figured out that the convergence in the x direction is slower than in y direction and thus, an increase of the number of \mathbf{k} points just in x direction (resulting in the set of 55 \mathbf{k} points) yields a strong improvement of the convergence. Comparing the spectra based on 25 and 55 \mathbf{k} points we have concluded that convergence has been already achieved with 25 \mathbf{k} points. Incidentally, using the Γ point only, a strong anisotropy appears (see inset of Fig. 6) which can be traced back to infinite chains in x direction of the bulk layers.⁷⁰

Since the slab thickness can influence the spectra, we

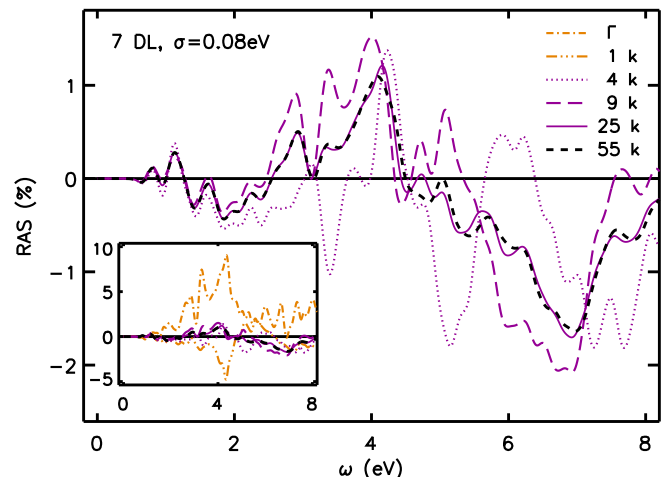


FIG. 6: (Color online): Convergence of the RAS of Si(113) 3×2 ADI with respect to the \mathbf{k} point summations. The 1 \mathbf{k} point sets (Γ and Baldereschi) are shown in the inset, since the corresponding RAS is larger by one order of magnitude. Convergence requires 25 \mathbf{k} points in the IBZ.

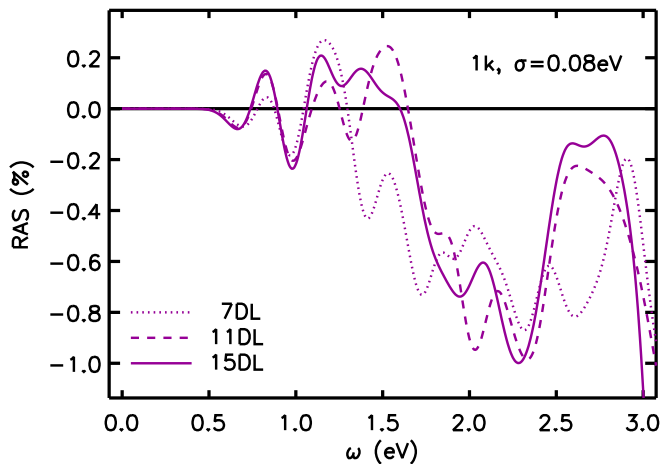


FIG. 7: (Color online): Convergence of the RAS of Si(113)3×2ADI with respect to the slab thickness (7 DL, 11 DL, 15 DL) using only the Baldereschi point in Eq. (1). Convergence is satisfactory using the 11 DL slab.

have calculated the RAS using only the Baldereschi⁷¹ point for various cell sizes, i.e. using slabs of 7 DL, 11 DL, and 15 DL. The 15 DL cell has been created by adding four bulk DL to the 11 DL slab. The outcome of the test is displayed in Fig. 7. It is clearly recognizable that the 7 DL slab does not describe the low energy region of the RAS correctly, where the differences between the 11 DL and the 15 DL cell are just minor ones. Hence, the use of the 11 DL cell produce reliable results for the surface spectra. Note that the spectra using only the Baldereschi point are not converged, but the use of just one point is sufficient for the check performed here. It has been already shown that the convergence regarding the thickness improves using more \mathbf{k} points.⁷² Concerning the \mathbf{k} -point convergence, we expect that our 25 \mathbf{k} -points set, which has been shown to be enough for the 7 DL slab, will also be at convergence for the 11 DL one.

B. Analysis of the RAS

We proceed now to analyze our fully converged RAS spectra (using the 11DL supercell and 25 \mathbf{k} points in the summation) with respect to the surface structure. Thus, we have performed a layer-by-layer decomposition as described in Refs. [66,73,74]. For this purpose, a real space cutoff has been used in order to separate the contributions coming from defined layers of the slab by introducing a boxcar function $\theta(z)$ in the calculation of the dipole matrixelements. The modified transition probability $\tilde{P}_{v\mathbf{k},c\mathbf{k}}^j$ can be rewritten as

$$\tilde{P}_{v\mathbf{k},c\mathbf{k}}^j = -i\hbar \int dr \psi_{v\mathbf{k}}^* \theta(z) \frac{\partial}{\partial r_j} \psi_{c\mathbf{k}} \quad (5)$$

and the summation of Eq. (1) changes to

$$\text{Im}[4\pi\alpha_{jj}^s(\omega)] = \frac{8\pi^2 e^2}{m^2 \omega^2 A} \sum_{\mathbf{k}} \sum_{v,c} \left[P_{v\mathbf{k},c\mathbf{k}}^j \right]^* \tilde{P}_{v\mathbf{k},c\mathbf{k}}^j \times \delta(E_{c\mathbf{k}} - E_{v\mathbf{k}} - \hbar\omega) \quad (6)$$

Note that only one of P and P^* must contain the θ function. The decomposed spectra are presented in Fig. 10 together with a side view of the slab. We have numbered the DL from the top to the bottom. For the analysis we have chosen three regions: The topmost two DL (DL01 and DL02 (surface), while DL00 is the vacuum layer above), the third and the fourth DL (subsurface, DL03 and DL04) where the optimization changed the atomic positions with respect to the bulk ones, and the bulk part together with the hydrogens (bulk, DL05 till DL11, while DL12 is the vacuum layer below), since the relaxation did not affect the atomic positions in DL05 and DL06.

In the low energy range of the spectra various peaks are visible. For further discussion we have labeled the low energy peaks with P1, P2, P3, P4, and P5 (see Fig. 10). Looking at the decomposed spectra in Fig. 8 one can see that the the peaks in the full spectra (containing the contribution of all DL) up to 2.5 eV (P1–P5) can be traced back to the surface and the subsurface DL, where the structures at higher energies are also bulk determined. Nevertheless, also at energies larger than 3 eV there exist surface related structures. However, these structures are due to surface-bulk, bulk-surface transitions and surface resonances. P1 and P3 originate from the surface layers only, whereas the peaks P2, P4, and P5 contain contributions from both the surface and the subsurface layers. Thus we can conclude that for an analysis of P1 and P3 only transitions between surface bands need to be considered, whereas for P2, P4, and P5 also resonances

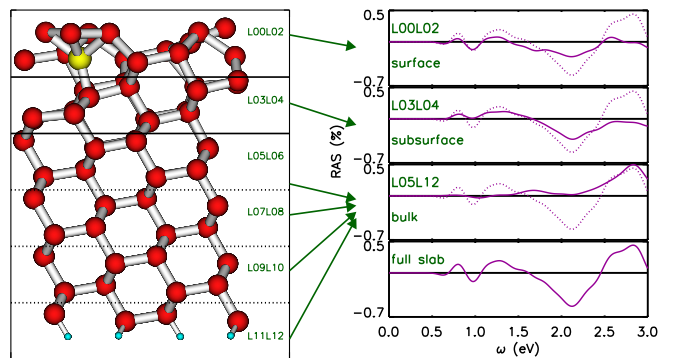


FIG. 8: (Color online): Side view of the 11 DL slab (left side) and layer-by-layer analysis of the RAS (right side). Besides the decomposed spectra (solid lines) also the full spectra (dotted lines in the upper three panels and solid line in the lower one on the right) is drawn for comparison. The arrows indicate where the contributions to the spectra come from. The DL assignment is explained in the text.

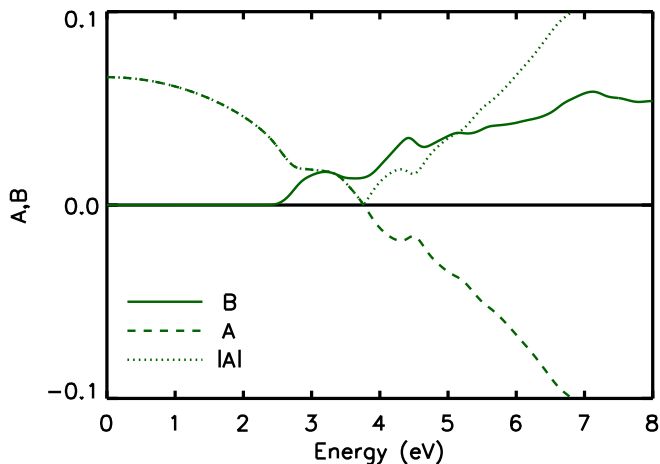


FIG. 9: (Color online): bulk coefficients A and B from Eq. (7). For energies smaller than 2.5 eV there is no contribution of $\text{Re}(4\pi\alpha^s)$ to the RAS.

or high-energy bulk states have to be investigated.

After identifying the surface peaks in the spectra, we want to identify the responsible transitions. Since for the deviation from the Fresnel reflectivity Eq. (3) the whole complex polarizability is considered, the RAS is also influenced by the real part of α . Thus, an overlap of spectral structures coming from the imaginary and the real part is possible. A feasible procedure for determining this overlap has been described in Ref. [75], where Eq. (3) was rewritten as

$$\frac{\Delta R_j}{R} = A \text{Im}[4\pi\alpha_{jj}^s] + B \text{Re}[4\pi\alpha_{jj}^s] \quad (7)$$

The energy-dependent coefficients A and B are determined only by the dielectric function of the bulk crystal. With the magnitude of A and B one can figure out if the RAS is mainly determined by $\text{Im}(4\pi\alpha^s)$ or by $\text{Re}(4\pi\alpha^s)$. In this way, A and B are surface independent coefficients.

Because of this, we analyzed these coefficients for our system, in detail, we determined A and B for bulk silicon. They are universal for all silicon surfaces, independent of the orientation and reconstruction. The result is shown in Fig. 9. Besides A and B , also $|A|$ is plotted in order to compare the magnitude of the coefficients. The result is the following: Every RAS of any clean silicon surface is determined only by $\text{Im}(4\pi\alpha^s)$ for an energy up to 2.5 eV and by both, $\text{Im}(4\pi\alpha^s)$ and $\text{Re}(4\pi\alpha^s)$, for higher energies. In detail, it is mainly determined by $\text{Im}(4\pi\alpha^s)$ for 2.5–3.2 eV, by both equally from 3.2–3.4 eV, mainly by $\text{Re}(4\pi\alpha^s)$ for 3.4–5.1 eV, and by $-\text{Im}(4\pi\alpha^s)$ for higher energies. Thus, the surface peaks P1–P5 can be traced back to the differences just between $\text{Im}(4\pi\alpha_{xx}^s)$ and $\text{Im}(4\pi\alpha_{yy}^s)$. These are the differences we investigate now in order to find the origin of the surface features in the RAS.

Since the RAS in the low-energy range (up to 1.3 eV, peaks P1 to P3) has been reproduced already sufficiently

well using the Baldereschi point only, based on this spectra the contribution of various transitions to the first three surface peaks has been analyzed. For the other spectral structures all \mathbf{k} points have been taken into account.

The first peak P1 of the RAS displayed in Fig. 10 appears due to the transition from the surface valence state S_0 to the surface conduction state C_1 . Considering the localization of the states (see Fig. 4), namely the position of the adatom 3, where the charge density of S_0 has been found, and that of the atoms 4-7-8 (the location of C_1) one sees that they are much nearer in y direction than in x . Therefore the transition probability in this case is higher for y polarized light, resulting in a negative RAS signal. Note that the transition from S_0 to C_2 is forbidden. Also the peak P2 in the RAS is due to transitions between surface bands: the transitions from S_1 to both the surface conduction bands C_1 and C_2 are responsible for it. Here, the distance between adatom 9 (S_1) and the filled pentagon 4-5-6-7-8 (C_1 and C_2) in x direction is small, where also a little overlap of the charge density appear. This yields in a strong positive signal in the RAS. Note that due to the overlap of S_1 with the bulk bands there is also a tiny contribution of bulk-surface transitions to P2. The peak P3 is determined by transitions from S_2 to C_1 and C_2 . The vicinity of the state S_2 , which is located at atoms 1-2-3, to the states C_1 and C_2 at the pentagon with interstitial (4-5-6-7-8) is mainly due to its localization at adatom 3. From the charge density localized at the atoms 1-2, for both polarizations the transition probability should be similar since the distances in x and y directions are equal. The additional localization at adatom 3 favor the y direction yielding the negative RAS signal. For the remaining two peaks P4 and P5 a mixture of bulk-surface and surface-bulk transitions (not restricted to single surface bands) is responsible, therefore a clear picture could not be drawn. The peaks P2 and P3 are equal in height, whereas P1 is a lower one. This might be due to the fact that for P2 and P3 transitions to two surface conduction states are responsible, but one of them is forbidden for P1. However, the overall magnitude of the probability of single transitions between surface bands is nearly the same in this case.

Considering the dispersion of the eigenenergies, the regions in the IBZ with the main contributions to the RAS have been identified using again a single- \mathbf{k} analysis⁷⁰: For P1, \mathbf{k} points near Γ carry the main contribution, whereas for P2 \mathbf{k} points close to the J-K boundary (large k_x component), and for P3 those close to the Γ -J boundary (small k_y component) comprise the main contributions. Such a trend has not been found neither for P4, nor for P5. A posteriori, due to this anisotropic distribution of the contribution, the convergence with respect to the \mathbf{k} points had to be expected to be a delicate one.

Changing the surface reconstruction certainly would affect the RAS. We can speculate that removing, e.g., the interstitial atom (atom 18) would change the local-

ization of the states C_1 and C_2 and which will have an effect to all three peaks discussed here. Adding an interstitial to the empty pentagon would affect mainly state S_2 , meaning the third peak in the spectra. Furthermore, having two nearly equivalent pentagons on the surface would influence the peak height, because the transition probability for the x and y would not be as significantly different as for the ADI reconstruction. However, also the energetic position of the surface peaks would indeed be affected.

C. Comparison with experimental results

Finally, in Fig. 10 we compare our RAS with the experimental data obtained by Aspnes and coworkers^{47,48}. Unfortunately, the measured RAS did not show any surface-related spectral structure. This might be due to passivation of the surface with Si-O suboxide. Thus, the theoretical surface peaks we have investigated cannot be compared. Regarding bulk-related structures, using a 11 DL slab does not allow the perfect description of the bulk derivative-like structure. In order to wash out artificial oscillations of bulk structures, we have applied a variable broadening. This means, we have employed a constant broadening for energies smaller than 2.5 eV (inset of the bulk spectra) and an additional broadening which goes linearly with the energy (factor 0.04) for higher energies. Furthermore, we scaled the measured RAS with a factor of 10, which is the usually accepted factor for silicon surfaces.⁷⁶ In this way we got a reasonable agreement with respect to our slab thickness in the medium energy range. As visible, the calculation reproduces the spectral

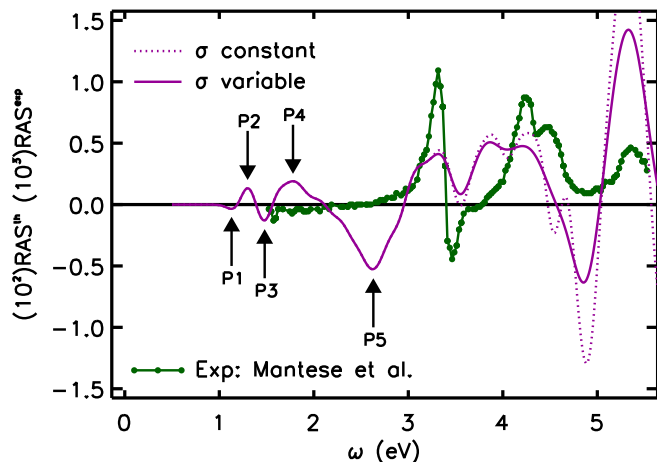


FIG. 10: (Color online): Comparison of the RAS calculated using 25 k points in the 11 DL cell (light curves) obtained with a constant broadening of 0.08 eV (dotted line) and a variable one (solid line), see text. The experimental spectra are from Refs. [47,48] (dark dots connected by a solid line). A scissor operator of 0.5 eV has been applied to the theoretical spectra, and the RAS amplitude has been scaled by a factor of 10 (see text).

structure at around 3.2 eV and the double peak at 4.2 eV, which is shifted slightly to lower energies in our case. Also the experimental structures at around 5 eV can be found in our spectra, however, it is a little bit overestimated. The bulk derivative-like structure itself at around 3.5 eV is reproduced only qualitatively, which is a result of the small slab size. Compared to the tight-binding calculation of Gavrilenko et al.⁵⁰, our spectra can resolve the characteristic low-energy surface peaks and describes the bulk derivative-like structure with the correct sign.

VI. SUMMARY AND CONCLUSIONS

In summary, we have investigated the electronic structure and the RAS spectrum of the Si(113) 3×2 ADI. The electronic band structure and the DOS were found in excellent agreement with available experimental results. We identified three surface valence bands and two surface conduction bands near the Fermi level by computing the wave function localization in the surface region. The valence surface states are located at the adatoms and at the pentagon without an interstitial, whereas the conduction surface states are located at the pentagon with an interstitial, in agreement with STM images. The three valence surface states in the energy gap compare with the two states which are visible in ARUPS¹⁸ and the ARPES^{15,16,64} experiments, where in the latter one a third surface (resonance) state has been found in overlap with the bulk states. Nevertheless, the existence of three surface valence states has been confirmed by the comparison of theoretical^{30,33,35,36} and experimental^{4,26,27,30,33,36} STM images and by a core-level analysis.^{15,16} Two of the valence surface states show a 3×2 and one a 3×1 periodicity, which has been confirmed experimentally.^{18,64} In addition, we found a surface state below the valence band minimum. This state is located at the filled pentagon and shows a Tamm-like character. This finding calls for more experimental work for measuring the DOS at low energy.

Concerning optical spectra, after checking the numerical convergence with respect to the slab thickness and the number of k points, we have performed a layer-by-layer spectral decomposition. In this way the surface-relevant spectral features have been determined. Furthermore, an analysis of the contributions of the real and the imaginary part of the polarizability lead to the conclusion that the surface relevant structures are due to the imaginary part only. We have traced back the first three low-energy peaks of the RAS to transitions from the three valence surface states S_0 , S_1 , and S_2 (localized at the adatoms and the empty pentagon) to both the conduction surface states, C_1 and C_2 (localized at the pentagon with interstitial). These RAS peaks are hence very sensitive to a change of the surface reconstruction. The missing splitting of the peaks in the RAS with respect to the two surface conduction states is assumed to be due to the small energy difference between them. The only available experimental RAS does not show any low-energy surface-

related spectral features, probably due to a surface contamination. At higher energy, the bulk-derivative like structure, as well as other spectral features, agree with those of the measured RAS. Differences with respect to the experimental results can be due to the limited size of the slab used in the calculations and to the negligence of self-energy and excitonic effects.

Acknowledgment

This work was funded by the EU's 6th Framework Programme through the NANOQUANTA Network of Excel-

lence (NMP4-CT-2004-500198). We would like to thank A. Incze, C. Hogan, and R. Del Sole for fruitful discussions. K. GN wants also to thank S. Hinrich for providing articles and additional information about the Si(113) surface. Computer facilities at CINECA granted by INFN (Project no. 352/2004 and no. 426/2005) are gratefully acknowledged.

-
- * Electronic address: katalin.gaal-nagy@physik.uni-r.de
- ¹ D. J. Eaglesham, A. E. White, L. C. Feldman, N. Moriya, and D. C. Jacobson, *Phys. Rev. Lett.* **70**, 1643 (1993).
 - ² H.-J. Müssig, J. Dąbrowski, and S. Hinrich, *Solid-State Electron.* **45**, 1219 (2001).
 - ³ H.-J. Müssig, J. Dąbrowski, K.-E. Ewald, P. Gaworzewski, A. Huber, and U. Lambert, *Microelectron. Eng.* **56**, 195 (2001).
 - ⁴ Z. Zhang, K. Sumitomo, H. Omi, T. Ogino, and X. Zhu, *Surf. Interface Anal.* **36**, 114 (2004).
 - ⁵ M. P. Halsall, H. Omi, and T. Ogino, *Appl. Phys. Lett.* **81**, 2448 (2002).
 - ⁶ Z. Zhang, K. Sumitomo, H. Omi, and T. Ogino, *Surf. Sci.* **497**, 93 (2002).
 - ⁷ K. Sumitomo, Z. Zhang, H. Omi, D. J. Bottomley, and T. Ogino, *J. Cryst. Growth* **237-239**, 1904 (2002).
 - ⁸ J. Knall and J. B. Pethica, *Surf. Sci.* **265**, 156 (1992).
 - ⁹ H. Omi and T. Ogino, *Phys. Rev. B* **59**, 7521 (1999).
 - ¹⁰ M. Hanke, T. Boeck, A.-K. Gerlitzke, F. Syrowatka, and F. Heyroth, *Appl. Phys. Lett.* **86**, 223109 (2005).
 - ¹¹ Y.-N. Yang, E. D. Williams, R. L. Park, N. C. Bartelt, and T. L. Einstein, *Phys. Rev. Lett.* **64**, 2410 (1990).
 - ¹² Y. R. Xing, J. P. Zhang, J. A. Wu, C. Z. Liu, and C. H. Wang, *Surf. Sci.* **232**, L215 (1990).
 - ¹³ H. Hibino and T. Ogino, *Phys. Rev. B* **56**, 4092 (1997).
 - ¹⁴ T. Suzuki, H. Minoda, Y. Tanishiro, K. Yagi, and ???, *Surf. Rev. Lett.* **5**, 249 (1998).
 - ¹⁵ C. C. Hwang, H. S. Kim, Y. K. Kim, K. W. Ihm, C. Y. Park, K. S. An, K. J. Kim, T.-H. Kang, and B. Kim, *Phys. Rev. B* **64**, 045305 (2001).
 - ¹⁶ C. C. Hwang, K.-J. Kim, T.-H. Kang, B. Kim, Y. Chung, and C. Y. Park, *Surf. Sci.* **514**, 319 (2002).
 - ¹⁷ K. Jacobi and U. Myler, *Surf. Sci.* **284**, 223 (1993).
 - ¹⁸ U. Myler and K. Jacobi, *Surf. Sci.* **220**, 353 (1989).
 - ¹⁹ Y.-N. Yang and E. D. Williams, *J. Vac. Sci. Technol. B* **8**, 2481 (1990).
 - ²⁰ S. M. Scholz and K. Jacobi, *Phys. Rev. B* **52**, 5795 (1995).
 - ²¹ C. C. Hwang, K. S. An, S. H. Kim, Y. K. Kim, C. Y. Park, S. N. Kwon, H. S. Song, K. H. Jung, T. Kinoshita, A. Kakizaki, et al., *J. Vac. Sci. Technol. A* **18**, 1473 (2000).
 - ²² H. Kim, T. Spila, and J. E. Greene, *Surf. Sci.* **490**, L602 (2001).
 - ²³ Z. H. Zhang, K. Sumitomo, and F. Lin, *Ultramicroscopy* **105**, 16 (2005).
 - ²⁴ Z. H. Zhang and K. Sumitomo, *Surf. Sci.* **576**, 83 (2005).
 - ²⁵ M. J. Hadley, S. P. Tear, B. Rottger, and H. Neddermeyer, *Surf. Sci.* **280**, 258 (1993).
 - ²⁶ J. Knall, J. B. Pethica, J. D. Todd, and J. H. Wilson, *Phys. Rev. Lett.* **66**, 1733 (1991).
 - ²⁷ H. Sakama, D. Kunitatsu, M. Kageshima, and A. Kawazu, *Phys. Rev. B* **53**, 6927 (1996).
 - ²⁸ C. Y. Chang, Y. C. Chou, and C. M. Wei, *Phys. Rev. B* **59**, R10453 (1999).
 - ²⁹ C. C. Hwang, H. S. Kim, Y. K. Kim, J. S. Kim, C. Y. Park, K. J. Kim, T.-H. Kang, and B. Kim, *Phys. Rev. B* **59**, 14864 (1999).
 - ³⁰ J. Dąbrowski, H.-J. Müssig, and G. Wolff, *Phys. Rev. Lett.* **73**, 1660 (1994).
 - ³¹ I. Takeguchi, M. Tanaka, H. Yasuda, and K. Furuya, *Surf. Sci.* **482-485**, 1385 (2001).
 - ³² M. Takeguchi, Y. Wu, and K. Furuya, *Surf. Interface Anal.* **30**, 288 (2000).
 - ³³ J. Dąbrowski, H.-J. Müssig, and G. Wolff, *J. Vac. Sci. Technol. B* **13**, 1597 (1995).
 - ³⁴ J. Dąbrowski, H.-J. Müssig, and G. Wolff, *Surf. Sci.* **331-333**, 1022 (1995).
 - ³⁵ A. A. Stekolnikov, J. Furthmüller, and F. Bechstedt, *Phys. Rev. B* **68**, 205306 (2003).
 - ³⁶ G.-D. Lee and E. Yoon, *Surf. Sci.* **559**, 63 (2004).
 - ³⁷ W. Ranke, *Phys. Rev. B* **41**, 5243 (1990).
 - ³⁸ K. A. Feng, X. M. Hu, Z. Lin, and Y. R. Xing, *Appl. Surf. Sci.* **120**, 94 (1997).
 - ³⁹ J. Wang, A. P. Horsfield, D. G. Pettifor, and M. C. Payne, *Phys. Rev. B* **54**, 13744 (1996).
 - ⁴⁰ K. S. Kim, J. U. Choi, Y. J. Cho, and H. J. Kang, *Surf. Interface Anal.* **35**, 82 (2003).
 - ⁴¹ G.-D. Lee and E. Yoon, *Phys. Rev. B* **68**, 113304 (2003).
 - ⁴² H. Ikeda, Y. Oshima, H. Hirayama, and K. Takayanagi, *Surf. Sci.* **433-435**, 632 (1999).
 - ⁴³ T. Suzuki, H. Minoda, Y. Tanishiro, and K. Yagi, *Surf. Sci.* **438**, 76 (1999).
 - ⁴⁴ A. A. Stekolnikov, J. Furthmüller, and F. Bechstedt, *Phys. Rev. B* **67**, 195332 (2003).
 - ⁴⁵ G.-H. Lu, M. Huang, M. Cuma, and F. Liu, *Surf. Sci.* **588**, 61 (2005).
 - ⁴⁶ U. Myler, P. Althainz, and K. Jacobi, *Surf. Sci.* **251-252**, 607 (1991).
 - ⁴⁷ L. Mantese, U. Rossow, and D. E. Aspnes, *Appl. Surf. Sci.* **107**, 35 (1996).
 - ⁴⁸ U. Rossow, L. Mantese, and D. E. Aspnes, *J. Vac. Sci.*

- Technol. B **14**, 3070 (1996).
- ⁴⁹ C. D. Hogan and C. H. Patterson, Phys. Rev. B **57**, 14843 (1998).
- ⁵⁰ V. I. Gavrilenko and F. H. Pollak, Phys. Rev. B **58**, 12964 (1998).
- ⁵¹ M. Palummo, G. Onida, R. DelSole, and B. S. Mendoza, Phys. Rev. B **60**, 2522 (1999).
- ⁵² P. Hohenberg and W. Kohn, Phys. Rev. **136 B**, 864 (1964).
- ⁵³ <http://www.abinit.org>.
- ⁵⁴ <http://users.unimi.it/etsf>.
- ⁵⁵ W. Kohn and L. J. Sham, Phys. Rev. **140 A**, 1133 (1965).
- ⁵⁶ D. M. Ceperley and B. J. Alder, Phys. Rev. Lett. **45**, 566 (1980).
- ⁵⁷ J. P. Perdew and A. Zunger, Phys. Rev. B **23**, 5048 (1981).
- ⁵⁸ N. Troullier and J. L. Martins, Phys. Rev. B **43**, 1993 (1991).
- ⁵⁹ G. F. Bassani, *Electronic states and optical transitions in solids* (Pergamon Press, Oxford, 1975).
- ⁶⁰ H. Ehrenreich and M. H. Cohen, Phys. Rev. **115**, 786 (1959).
- ⁶¹ R. DelSole and R. Girlanda, Phys. Rev. B **48**, 11789 (1993).
- ⁶² R. DelSole, in *Photonic Probes of Surfaces*, edited by P. Halevi (Elsevier, Amsterdam, 1995), p. 131.
- ⁶³ H. J. Monkhorst and J. D. Pack, Phys. Rev. B **13**, 5188 (1976).
- ⁶⁴ K. S. An, C. C. Hwang, H. S. Kim, C.-Y. Park, I. Matsuda, H. W. Yeom, S. Suga, and A. Kakizaki, Surf. Sci. **478**, 123 (2001).
- ⁶⁵ W. Arabczyk, H.-J. Mussig, J. Dąbrowski, D. Moszynski, and S. Hinrich, Appl. Surf. Sci. **135**, 59 (1998).
- ⁶⁶ C. Hogan, R. DelSole, and G. Onida, Phys. Rev. B **68**, 035405 (2003).
- ⁶⁷ I. Tamm, Phys. Z. Sowjetunion **1**, 733 (1932).
- ⁶⁸ K. C. Pandey, T. Sakurai, and H. D. Hagstrum, Phys. Rev. Lett. **35**, 1728 (1975).
- ⁶⁹ K. C. Pandey, J. Vac. Sci. Technol. **15**, 440 (1978).
- ⁷⁰ K. Gaál-Nagy and G. Onida, in *Epioptics-9*, edited by A. Cricenti (Work Scientific, Singapore, in press).
- ⁷¹ A. Baldereschi, Phys. Rev. B **7**, 5212 (1973).
- ⁷² R. DelSole and G. Onida, Phys. Rev. B **60**, 5523 (1999).
- ⁷³ C. Castillo, B. S. Mendoza, W. G. Schmidt, P. H. Hahn, and F. Bechstedt, Phys. Rev. B **68**, 041310(R) (2003).
- ⁷⁴ P. Monachesi, M. Palummo, R. DelSole, A. Grechnev, and O. Eriksson, Phys. Rev. B **68**, 035426 (2003).
- ⁷⁵ C. Hogan and R. DelSole, Phys. Stat. Sol. (b) **242**, 3040 (2005).
- ⁷⁶ A. Incze, G. Onida, R. DelSole, F. Fuchs, and Y. Borenzstein, preprint (2006).